Inorganic Chemistry
Cite This: Inorg. Chem. 2018, 57, 11146−11156
Article
pubs.acs.org/IC

Removal of A-Site Alkali and Alkaline Earth Metal Cations in $KBe_2BO_3F_2$-Type Layered Structures To Enhance the Deep-Ultraviolet Nonlinear Optical Capability

Lei Kang,[†,‡] Zheshuai Lin,[*,∥] Feng Liu,[*,‡] and Bing Huang[*,†]

[†]Beijing Computational Science Research Center, Beijing 100193, China
[∥]Technical Institute of Physics and Chemistry, Chinese Academy of Sciences, Beijing 100190, China
[‡]Department of Materials Science and Engineering, University of Utah, Salt Lake City, Utah 84112, United States

Supporting Information

ABSTRACT: In order to generate deep-ultraviolet (DUV, λ < 200 nm) coherent light, many DUV-transparent nonlinear optical (NLO) compounds have been synthesized experimentally over the past few decades, most of which contain alkali or/and alkaline earth metal cations. However, to date, practical DUV NLO materials beyond $KBe_2BO_3F_2$ (KBBF) are still very scarce. In this work, based on analysis of the DUV NLO effect induced by the A-site alkali and alkaline earth metal cations, we attempt to expand the options for DUV NLO compounds from a molecular engineering point of view. Accordingly, a useful strategy is proposed to design densely stacked layered structures without A-site cations as new and promising DUV NLO materials. Along with the available experimental and first-principles calculation results, it is demonstrated that layered structures in which the A-site cations are removed, such as Be_2BO_3F, $Be_2CO_3F_2$, $AlCO_3F$, $SiCO_3F_2$, $AlNO_3F_2$, PBO_3F_2, and $PB_3O_6F_2$, whether real or hypothetical, exhibit excellent DUV NLO performances. Based on the findings, our strategy may open up new opportunities for the design and exploration of high-performance DUV NLO materials beyond KBBF.

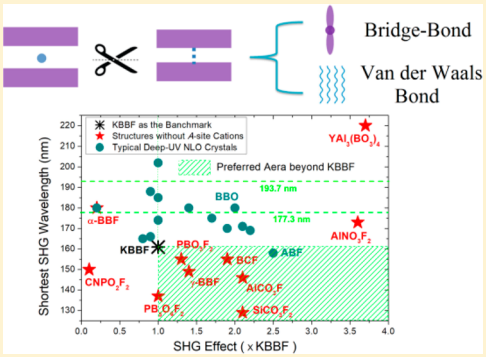

1. INTRODUCTION

Deep-ultraviolet (DUV) nonlinear optical (NLO) crystals are of great importance for current and future fundamental research and technical needs associated with all-solid-state lasers.[1,2] Short laser output wavelength and high conversion efficiency are the most important requirements for a DUV NLO material in the practical second harmonic generation (SHG).[3] In principle, the short output wavelength requires a phase-matching (PM) output $\lambda_{PM} \leq 200$ nm rather than a DUV absorption edge $\lambda_{UV} \leq 200$ nm. Accordingly, a good DUV NLO crystal must have (i) an appropriate λ_{UV}, at least ≤200 nm and ≤177.3 nm when applied in the sixth harmonic generation (6HG) of the most practical 1064 nm Nd:YAG laser, and (ii) a sufficient PM capability, usually corresponding to large birefringence, $\Delta n \geq 0.07$, and suitable refractive dispersion in the UV and DUV regions.[4] Furthermore, high NLO conversion efficiency needs (iii) a large effective SHG effect d_{eff}, mainly corresponding to the large SHG coefficients $|d_{ij}|_{max} \geq d_{36} = 0.39$ pm/V of KH_2PO_4 (KDP) in the PM direction, and the larger the better. Only when conditions (i), (ii), and (iii) are satisfied could DUV coherent light be output through the NLO crystal.

However, it is difficult to achieve such conditions for most conventional structures, which results in DUV NLO materials being very rare.[5,6] As the rare and first exception to break the "200-nm-wall", $KBe_2BO_3F_2$ (KBBF) satisfies the requirements very well, with $\lambda_{UV} = 150$ nm, $\Delta n = 0.088$ (default at 400 nm), and $d_{16} = 0.5$ pm/V, so its λ_{PM} can reach 161 nm.[7] The excellent DUV NLO capability comes from KBBF's unique structural features. First, its two-dimensional (2D) $(Be_2BO_3F_2)_\infty$ layered framework exhibits strong spatial anisotropy for a sufficiently large Δn. Meanwhile, all $(BO_3)^{3-}$ are planar and aligned in the same orientation, resulting in an available SHG effect. Importantly, each Be^{2+} is saturated with the nonbonding states of dangling O^{2-} in $(BO_3)^{3-}$, so the energy bandgap E_g is sufficiently enlarged, corresponding to a greatly reduced λ_{UV}.[4] However, the interlayer connection is not strong and there is a lack of covalent directionality due to the A-site alkali metal cations K^+ located between $(Be_2BO_3F_2)_\infty$ layers, so KBBF exhibits a heavy layering tendency during the growth of single crystals.[8] Until now, the thickness of KBBF with good optical quality was less than 4 mm along the crystal c-axis, which strongly hinders its industrial and commercial applications. In addition, an effective SHG coefficient is available but still relatively small (only ∼1.2 times that of KDP), which makes its SHG conversion efficiency not high enough, so it has only achieved a 177.3 nm laser with 200 mW, still below the watt level.[9] Considering the demand for DUV NLO devices and the lack of good KBBF crystals, it is

Received: June 21, 2018
Published: August 15, 2018

DOI: 10.1021/acs.inorgchem.8b01712
Inorg. Chem. 2018, 57, 11146−11156

imperative to search for new DUV NLO materials beyond KBBF to replace it.

In the past few decades, researchers have been looking for new DUV NLO materials.[10−37] In general, some of these materials do have possible DUV properties, but most are not better than KBBF. For example, as typical KBBF-family members, $RbBe_2BO_3F_2$ (RBBF)[10] and $CsBe_2BO_3F_2$ (CBBF)[11] exhibit inferior DUV capabilities compared to KBBF because Δn decreases with the increase of A-site cationic size from K^+ to Rb^+ and Cs^+, so the PM ability is weakened from KBBF to RBBF and CBBF.[38] For this reason, CBBF ($\lambda_{PM} \approx 202$ nm) cannot be used for DUV generation, although its λ_{UV} is 150 nm, and the effective SHG effect d_{eff} of RBBF along the PM direction is only half that of KBBF, although its d_{16} is close to that of KBBF. In the KBBF-type systems, no matter which kind of A-site cations are adopted, e.g., $NaBe_2BO_3F_2$ (NBBF),[39] $BaBe_2BO_3F_3$,[40] $NaCaBe_2B_2O_6F$,[18] $NaSr_3Be_3B_3O_9F_4$,[16] $BaAlBO_3F_2$,[12] $Rb_3Al_3B_3O_{10}F$,[23] etc., the obtained structures do not exhibit superior or comparable DUV PM capabilities compared to KBBF. In this sense, KBBF was once considered to approach the "DUV NLO limit" for the first generation.[41] However, in fact, the DUV NLO capability in the KBBF-family structure can be further enhanced in an extreme case with a zero cationic size, i.e., by removal of the A-site cations, which has not been systematically considered in the previous studies.

Therefore, in this work, we illustrate that the NLO size effect induced by the A-site alkali and alkaline earth metal cations plays an important role in the DUV NLO capability. Based on understanding of structure−property relationships, we attempt to break the DUV NLO limit beyond the KBBF system. Accordingly, we propose a useful strategy to design new DUV NLO crystals through densely stacked layered connections without A-site cations, and we further evaluate the DUV NLO capabilities of some known and designed structures using high-precision computational simulations. Note that this is a more effective way to produce new structures with excellent DUV NLO performances than any previous strategy. Therefore, we give an optimistic outlook for new and promising DUV NLO candidates beyond KBBF, which could be very beneficial for finding new NLO materials in the DUV region in the future.

2. RESEARCH METHODS

Looking back at the findings on KBBF, the *ab initio* algorithm combined with the anionic group theory gave much insight toward understanding the optical response from anionic groups in borate-based NLO crystals.[4] The density functional theory (DFT) energy-band method was developed to calculate the macroscopic SHG coefficients using high-performing computers.[42] It is apparent that the DFT calculations have achieved remarkable success in obtaining NLO properties and in elucidating the relationship between macro-NLO capability and microstructures. Compared with traditional experimental methods based on time-consuming trial-and-error study, NLO material scientists are willing to subsume themselves in a reasonable, controllable, and convenient effort to search for and even design the new functional NLO structures. To meet this objective, a theoretical approach provides efficient benefits for evaluating and determining the DUV NLO performance characteristics, such as the SHG effect, birefringence, energy bandgap, and PM output wavelength, of known and designed NLO structures.[43]

The present calculations in this work are performed by using the plane wave pseudopotential method implemented in the CASTEP package.[44,45] Optimized norm-conserving pseudopotentials are adopted for all elements.[46] A series of computational parameters with high precision are chosen for the calculations, including a kinetic energy cutoff of 1000 eV, a self-consistent field (SCF) tolerance of 5.0×10^{-9} eV/atom, and Monkhorst−Pack k-point meshes spanning less than 0.04 $Å^{-3}$ in the Brillouin zone.[47] The unit cell parameters and atomic positions are optimized using the quasi-Newton method.[48] The convergence thresholds between optimization cycles for energy change, maximum force, maximum stress, and maximum displacement are set as 5.0×10^{-6} eV/atom, 0.01 eV/Å, 0.02 GPa, and 5.0×10^{-4} Å, respectively. Based on the optimized structures and ground-state calculations, the electronic structures and optical properties can be obtained according to our proposed methods.[43] Accordingly, the energy bandgap E_g is calculated from the hybrid PBE0 functional,[49] while the optical properties are calculated by the scissors-corrected GGA method with PBE functional,[50] where the scissors operator is set as the difference between the PBE0 and PBE bandgaps.[51] This self-consistent *ab initio* approach has proven to be an efficient way to study the DUV NLO properties in many materials without introducing any experimental parameter (for details, see the Supporting Information).[43] As a result, the refractive indices n and birefringence Δn are obtained. The shortest SHG output wavelength λ_{PM} can be indicated on the basis of the dispersion curves of refractive indices (e.g., n_o and n_e), satisfying the condition of $n_o(2\lambda_{PM}) = n_e(\lambda_{PM})$. Further, the SHG coefficients d_{ij} are calculated using the expressions developed by our group.[42] Finally, the effective SHG coefficients d_{eff} can be simulated under the specific PM process.

Note that the proposed calculations are more efficient than conventional techniques. For accurate experimental measurements of DUV bandgap, SHG coefficients, and refractive indices, bulk crystals with large size and good optical quality are necessary. It is not easy to obtain large crystals, which hinders the determination of NLO performances. Although a rough experiment can provide some preliminary results, the evidence is insufficient or even may have large errors in some cases (e.g., powder SHG effect). According to our proposed studies, now we can accurately calculate the energy bandgap E_g, SHG coefficients d_{ij}, birefringence Δn, and the shortest SHG output λ_{PM}, all of which are the most important indexes for the DUV NLO crystals. Therefore, it is very important to perform appropriate calculations for adequate evaluations. Furthermore, if the designed structure exhibits a potential DUV NLO capability, it is necessary to evaluate the structural stability for its possible experimental synthesis. Theoretically, the first-principles linear response method is used to obtain the phonon dispersion of the crystal,[52] which can be used to analyze the structural stability.[53] The structure is dynamically stable without any virtual frequency. Meanwhile, first-principles molecular dynamics (MD) simulations can be performed to confirm that the lattice structure is stable at high temperatures. If the structures are maintained after a long MD simulation, they can be used as practical devices with stable electronic and optical properties. Under this research framework, two NLO compounds, $NH_4Be_2BO_3F_2$ (ABBF) and γ-Be_2BO_3F (γ-BBF), have been previously predicted and successfully obtained in recent experiments.[34,35]

3. RESULTS AND DISCUSSION

3.1. NLO Size Effect Induced by the A-Site Cations in the KBBF-Family Crystals. The so-called A-site cations herein are substantially spherical cations which are relatively isolated and have little covalent anisotropy, mainly including the alkali metals (e.g., Li^+, Na^+, K^+, Rb^+, Cs^+) and alkaline earth metals (e.g., Mg^{2+}, Ca^{2+}, Sr^{2+}, Ba^{2+}). In general, they do not directly affect the overall NLO response since the NLO effect or birefringence of a crystal is derived from the geometrical anisotropy of anionic groups based on the anionic group theory.[5] However, the spherical A-site cations can adjust the size of the stable structures and the arrangement of microscopic polar units, thereby indirectly affecting the final stability and NLO capability. This can be illustrated by the typical KBBF-family members, i.e., RBBF,[10] CBBF,[11] NBBF,[39] ABBF,[34] and $TlBe_2BO_3F_2$ (TBBF),[54] with structures similar to that of KBBF (see Figure S1 in the Supporting Information).

DOI: 10.1021/acs.inorgchem.8b01712
Inorg. Chem. 2018, 57, 11146−11156

Table 1. Experimental and Calculated NLO Properties of Typical KBBF-Family Crystals

		SG	E_g (eV)	λ_{UV} (nm)	d_{ij} (pm/V)	Δn at 400 nm	λ_{PM} (nm)
LBBF#[a]	calc	*R*32	8.38	148	$d_{16} = -d_{22} = 0.46$	0.067	165
NBBF#	calc	*R*32	8.11	153	$d_{16} = -d_{22} = 0.44$	0.064	170
NBBF	expt	*C*2	8.07	154	~KDP	–	–
	calc		8.26	151	$d_{23} = 0.44$	0.059	185
KBBF	expt	*R*32	8.45	147	$d_{16} = -d_{22} = 0.47$	0.088	161
	calc		8.31	150	$d_{16} = -d_{22} = 0.41$	0.059	172
ABBF	expt	*R*32	8.12	153	~1.2 × KDP	0.078	174
	calc	*R*3	8.37	149	$d_{16} = -d_{22} = 0.40$ $d_{33} = 0.23$	0.053	188
RBBF	expt	*R*32	8.18	152	$d_{16} = -d_{22} = 0.45$	0.078	174
	calc		8.21	151	$d_{16} = -d_{22} = 0.40$	0.057	185
CBBF	expt	*R*32	8.23	151	$d_{16} = -d_{22} = 0.50$	0.064	202
	calc		8.23	151	$d_{16} = -d_{22} = 0.38$	0.055	200
TBBF	expt	*R*32	≥6.3	≤200	~KDP	–	–
	calc		6.58	189	$d_{16} = -d_{22} = 0.46$	0.044	330

[a]Here, throughout the text, and in other tables, # indicates that the compound is designed theoretically.

Note that the A-site cations Rb^+, Cs^+, Na^+, Tl^+, and NH_4^+ are located between $(Be_2BO_3F_2)_\infty$ layers, like K^+ in KBBF. Their crystallographic data are given in Table S1 in the Supporting Information. It can be seen that the $(BO_3)^{3-}$ units maintain almost the same size $d_{B\text{-}O}$ in all crystals, while $d_{Be\text{-}F}$ in $(BeO_3F)^{5-}$ is slightly elongated with the increase of A-site cationic size $d_{A\text{-}F}$ (i.e., the distance between A-site cations and adjacent F anions). The interlayer distance d_{int}, $2d_{A\text{-}F}$, and volume with respect to the effective radius of A-site cations are further plotted in Figure S2 in the Supporting Information, in which the proportional change is easy to understand when the isolated cations and anionic groups are densely stacked.

Their NLO properties are listed in Table 1, showing a quantitative agreement between experimental and calculated E_g, λ_{UV}, d_{ij}, Δn, and λ_{PM}. Note that the shortest SHG output wavelength λ_{PM} is mainly determined by the optical birefringence Δn when λ_{UV} is sufficiently short, i.e., λ_{PM} generally decreases as Δn increases (see Figure 1a). In order to show the influence of A-site cations on the DUV NLO capability, two new structures, $LiBe_2BO_3F_2$ (LBBF) and NBBF#, with the same space group *R*32 as KBBF, are designed theoretically to enrich the KBBF-family. Their λ_{PM} values are plotted as a function of A-site cationic size $d_{A\text{-}F}$ in Figure 1b, exhibiting a proportional relation between λ_{PM} and $d_{A\text{-}F}$ for LBBF, NBBF#, KBBF, RBBF, ABBF, and CBBF. With the increase of the ionic radius, the crystal size along the *c*-axis increases, while in the *a*−*b* plane it is almost unchanged, so the refractive index along the *c*-axis (i.e., n_e) increases while that in the *a*−*b* plane (i.e., n_o) is almost constant. Therefore, the uniaxial birefringence $\Delta n = n_o - n_e$ is decreased from LBBF to CBBF, such that the PM ability is weakened successively. This is the so-called "NLO size-effect" induced by the A-site cations, which can also be inferred from the anionic group theory.[5,38] According to the theorem, increasing size perpendicular to $(BO_3)^{3-}$ plane groups will reduce the Δn, thus leading to the phase-mismatch in the DUV region and a decrease in the effective SHG effect. It should be explained that, for TBBF, E_g and Δn are relatively small because covalent Tl^+ has a nonbonding lone electron pair and is not a strictly spherical cation (see Figure S3 in the Supporting Information). For NBBF, the NLO-active $(Be_3B_3O_6F_3)_\infty$ layer slips and deviates from the structure expected based on KBBF, so the refractive dispersion becomes heavy, which makes its λ_{PM} only about 185 nm, red-shifted 15 nm compared to the expected NBBF# structure (~170 nm).

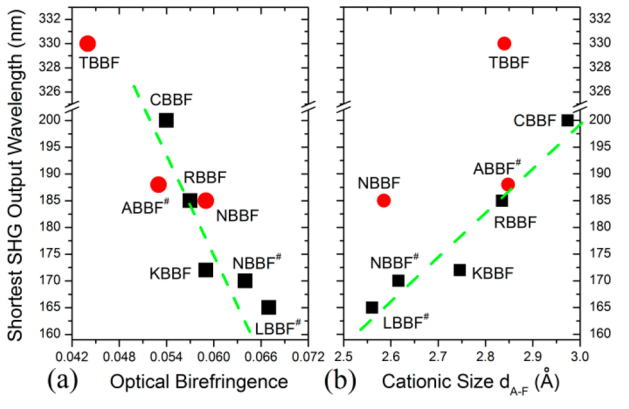

Figure 1. Shortest SHG wavelength λ_{PM} with respect to birefringence Δn (a) and A-site cationic size $d_{A\text{-}F}$ (b).

3.2. New Design Strategy for Removing the A-Site Cations in Layered Structures. Depending on the NLO size-effect induced by the A-site cations, it is conceivable to devise an important and simple design strategy to enhance the DUV NLO capability in the KBBF-like layered structures, i.e., to reduce the A-site cationic size to zero by removing the A-site cations. However, based on a thorough survey of the Inorganic Crystal Structure Database (ICSD, FIZ Karlsruhe, 2018, Version 3.7.0), there are no expected layered structures in

DOI: 10.1021/acs.inorgchem.8b01712
Inorg. Chem. 2018, 57, 11146−11156

which the A-site cations are removed. Table 2 lists the NLO properties of all 12 typical known DUV transparent oxides

Table 2. NLO Properties of Typical Oxides without A-Site Cations As Found in the ICSD

		λ_{UV} (nm)	$\lvert d_{ij}\rvert_{max}$ (pm/V)	Δn at 400 nm	λ_{PM} (nm)
BPO_4	expt	134	d_{36} = 0.76	0.006	N/A
	calc	134	d_{36} = 0.72	0.011	N/A
SiP_2O_7	calc	163	d_{33} < 0.01	0.013	N/A
$P_4O_4F_6$	calc	171	d_{11} = 0.13	0.025	N/A
$CNPO_2F_2$	calc	158	d_{31} = 0.06	0.139	~158
$YAl_3(BO_3)_4$	expt	166	d_{11} = 1.70	0.068	<266
	calc	155	d_{11} = 1.46	0.062	~220
$YBe_2B_5O_{11}$	expt	≤200	0.9×KDP	–	–
	calc	167	d_{33} = 0.23	0.016	N/A
$Y_2Be_2SiO_7$	calc	174	d_{11} = 0.15	0.029	N/A
$Y_2SiP_4O_{15}$	calc	174	d_{36} = 0.09	0.045	>266
YCO_3OH	calc	173	d_{36} = 0.49	0.057	>266
Al_5BO_9	calc	176	d_{36} = 0.20	0.016	N/A
BeP_2O_6	calc	166	d_{36} = 0.30	0.017	N/A
α-BBF	expt	≤186	0.3×KDP	–	–
	calc	148	d_{15} = 0.02	0.077	~180

without the A-site cations. It can be seen that BPO_4,[55] SiP_2O_7,[56] $P_4O_4F_6$,[57] $Y_2SiP_4O_{15}$,[58] $YBe_2B_5O_{11}$,[21] $Y_2Be_2SiO_7$,[59] Al_5BO_9,[60] and BeP_2O_6[61] are unlikely to achieve the DUV PM output due to their relatively small birefringence (Δn < 0.05). The reason is the small structural anisotropy of the NLO-active tetrahedral or octahedral anionic units (see Figure S4 in the Supporting Information), which results in a small optical anisotropy of the entire system. If planar NLO-active units such as $(BO_3)^{3-}$ or $(CO_3)^{3-}$ are introduced, the optical anisotropy will be enlarged, as in the cases of $YAl_3(BO_3)_4$ and YCO_3OH with $\Delta n \approx 0.07$ and 0.06, respectively.[62,63]

If the structural anisotropy is further enlarged by forming 1D chains or 2D layers, the DUV PM conditions may be satisfied as in the cases of $CNPO_2F_2$ and Be_2BO_3F (α-BBF).[64,65] Actually, $CNPO_2F_2$ with isolated CNO-POF_2 chains exhibits strongly anisotropic polarity so that it is predicted to be a DUV birefringent crystal with $\Delta n \approx 0.14$ and can achieve the PM output up to 158 nm, close to that of KBBF (~161 nm).[64] However, the polar CNO-POF_2 molecules are not arranged in a polarity-parallel manner so that the total SHG effect is very small (only ~1/10 × KBBF). Therefore, it is not a promising DUV NLO material unless the NLO-active molecules can be aligned in the same orientation. Similarly, α-BBF exhibits a sufficiently large Δn (~0.077) and available DUV λ_{PM} (~180 nm),[65] but the total SHG effect of this compound is small too, only ~1/5 × KBBF, due to the polarity-nonparallel arrangement of $(BO_3)^{3-}$ groups (see Figure 2a). Therefore, the

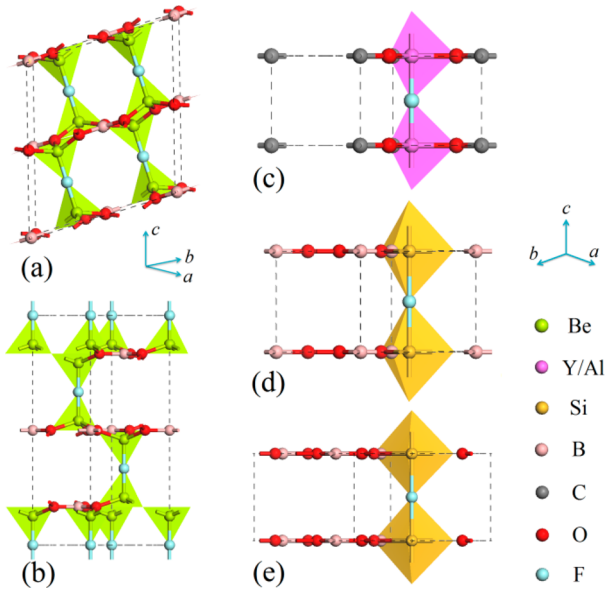

Figure 2. Crystal structures of α-BBF (a), γ-BBF (b), YCO_3F/$AlCO_3F$ (c), $SiBO_3F$ (d), and SiB_3O_6F (e).

difficulty of these compounds unsuitable as DUV NLO materials lies in the facts that (1) they are not largely anisotropic systems, so their Δn are not large enough, and (2) they are not polarity-parallel structures, so their total SHG effects are very small. In the following, we will investigate this difficulty to see if the DUV NLO capability is enhanced by forming the layered structures without A-site cations.

3.2.1. Bridge-Bonded Layered Structures without A-Site Cations. From the above analysis, the known α-BBF phase is derived from KBBF by removing one K^+ cation and one F^- anion. At the same time, the rest F^- anions are directly connected to the adjacent $(Be_2BO_3F_2)_\infty$ layers as bridge ions rather than dangling ions (see Figure 2a).[65] Moreover, if the $(BO_3)^{3-}$ in Be_2BO_3F can be arranged in a parallel manner as shown in Figure 2b, the total SHG effect will be greatly improved.[34] This can be seen from the calculations in Table 3 that the birefringence and SHG effect of the designed Be_2BO_3F (γ-BBF) are approximately 0.10 at 400 nm and 1.5 times that of KBBF, respectively. Thus, the shortest SHG PM wavelength λ_{PM} can reach 149 nm, blue-shifted about 12 nm compared to

Table 3. NLO Properties of γ-BBF, YCO_3F, $AlCO_3F$, $SiBO_3F$, and SiB_3O_6F

		λ_{UV} (nm)	d_{ij} (pm/V)	Δn at 400 nm	λ_{PM} (nm)
γ-BBF	expt	≤200	~2.3 × KDP	–	–
	calc	140	d_{12} = 0.63	0.094	149
$YCO_3F^{\#}$	calc	168	d_{11} = 2.62	0.197	168
$AlCO_3F^{\#}$	calc	146	d_{11} = 0.64 d_{22} = 0.98	0.153	146
$SiBO_3F^{\#}$	calc	144	d_{11} = 0.35 d_{22} = 0.69	0.083	165
$SiB_3O_6F^{\#}$	calc	146	d_{11} = 0.73 d_{22} = 0.58	0.107	146

DOI: 10.1021/acs.inorgchem.8b01712
Inorg. Chem. 2018, 57, 11146−11156

that of KBBF (~161 nm).[34] Importantly, this compound was obtained experimentally and recently reported,[35] with a good agreement between the experimental results and our calculations. This proves to some extent that the effectiveness of our research methods using the DFT simulations is guaranteed. Moreover, the F-bridge-bonded layered structure can enhance the interlayer connection compared to ionic-bonded KBBF structure, so it might improve the crystal growth behavior along the *c*-axis, which is important for the practical applications with large-size crystals. Of course, other phases can also be designed accordingly (e.g., Be_2BO_3F with the space group $P\bar{6}2c$),[66] although the related experiments have not been reported.

In fact, we can also construct similar Be-free systems, such as YCO_3F, $AlCO_3F$, $SiBO_3F$, and SiB_3O_6F, all of which exhibit structural features of the polar F-bridge-bonded layered frameworks as shown in Figure 2 (for detailed crystallographic data, see Table S2 in the Supporting Information). Specifically, YCO_3F was designed to expand the structural anisotropy of the known YCO_3OH in Table 2.[63] Note that the total SHG effect and birefringence are indeed enlarged, respectively from 1.3 to 6.5 × KDP and 0.06 to 0.19 as shown in Table 3. Consequently, YCO_3F has been able to achieve the DUV PM output of 168 nm below the practical 177.3 nm with very high conversion efficiency (6.5 × KDP is a very large SHG effect in the DUV materials). In addition, if the coordinated Y^{3+} can be replaced by Al^{3+}, the energy bandgap E_g (λ_{UV}) of the resulting $AlCO_3F$ will be greatly increased (decreased) so that the shortest DUV SHG output wavelength λ_{PM} can be blue-shifted from 168 to 146 nm. Although the SHG effect and birefringence are reduced to 1 pm/V and 0.15, they are still sufficient for the DUV NLO generation. Similarly in the borate-based system, $SiBO_3F$ and SiB_3O_6F are proposed to exhibit larger energy bandgaps ($E_g \approx 8.6$ and 8.5 eV) and stronger SHG effect ($|d_{ij}|_{max} \approx 1.5 \times$ KBBF) than KBBF by the combination of $(SiO_3F_2)^{4-}$ and $(BO_3)^{3-}$ or $(B_3O_6)^{3-}$. Moreover, the birefringence of $SiBO_3F$ ($\Delta n \approx 0.08$) is as large as KBBF, corresponding to the λ_{PM} (~165 nm) close to KBBF (~161 nm), and that of SiB_3O_6F ($\Delta n \approx 0.11$) is larger than KBBF so that it can output shorter SHG wavelength ($\lambda_{PM} \approx 146$ nm). All analysis show that the polar F-bridge-bonded layered structures without A-site cations actually facilitate superior DUV NLO capabilities, resulting in the DUV PM outputs with strong SHG effects.

3.2.2. van der Waals (vdW)-Connected Layered Structures without A-Site Cations. In fact, there is another proposal to form densely stacked layered frameworks without A-site cations, the key to which is to introduce the vdW interaction so that adjacent monolayers can be densely stacked. This proposal has never been mentioned in details before this work. Using this proposal in a simple way, the kind of vdW-connected layered structures without A-site cations can be designed according to the structural evolution as demonstrated in Figure 3a. Therein, we introduced a carbonate-based $(Be_2CO_3F_2)_\infty$ layered structure instead of borate-based $(Be_2BO_3F_2)_\infty$ of KBBF while removing the K^+ cations between layers. The resulting $Be_2CO_3F_2$ (BCF) crystal is likely to have an excellent DUV NLO capability since the $(Be_2CO_3F_2)_\infty$ framework exhibits relatively large structural anisotropy (i.e., large Δn), polarity-parallel arrangement (i.e., large d_{ij}) and few nonbonding states (i.e., large E_g). Considering that a large number of vdW materials have been grown with large crystal size, the dense interlayer vdW connection might exhibit more suitable growth than KBBF. Therefore, it is reasonable for us to believe that our proposed BCF may be a promising DUV NLO system with both favorable DUV output and growth capabilities.

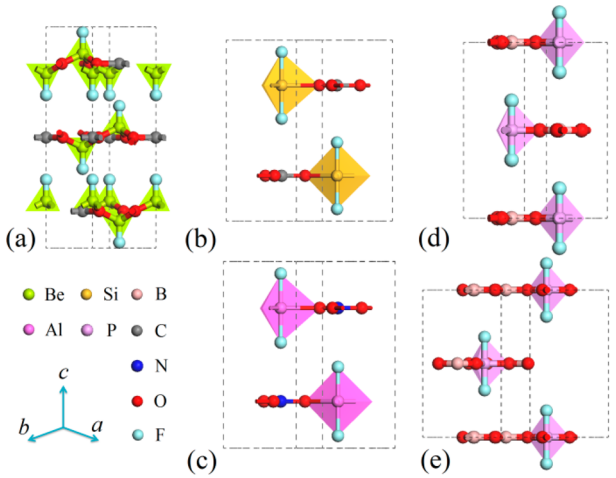

Figure 3. Crystal structures of BCF (a), $SiCO_3F_2$ (b), $AlNO_3F_2$ (c), PBO_3F_2 (d), and $PB_3O_6F_2$ (e).

It must be emphasized that the vdW interaction plays a dominant role between the $(Be_2CO_3F_2)_\infty$ layers, which is different from the $(Be_2BO_3F_2)_\infty$ layers in KBBF. Since there are no interlayer atoms, the interlayer distance in BCF is reduced to 4.7 Å from 6.2 Å in KBBF. It is the dense-stacking vdW connection between layers that determines better DUV NLO capability of BCF than that of KBBF, which can be found from the DFT results in Table 4. It is clearly seen that (1) BCF can be transparent for the DUV light above 148 nm close to KBBF; (2) it exhibits a strong SHG effect with $d_{11} \approx 2.1 \times$ KBBF; and (3) the birefringence ($\Delta n \approx 0.11$) is larger than that of KBBF (~0.088), to be large enough and very moderate for the DUV PM condition. Therefore, the shortest SHG output wavelength λ_{PM} is blue-shifted by about 6 nm from KBBF (~161 nm) to BCF (~155 nm). Moreover, its uniaxial birefringence is beneficial to the actual applications as a NLO or birefringent material. The results demonstrate that BCF is a promising vdW-connected layered structure with DUV NLO capability superior to KBBF.

Table 4. NLO Properties of BCF, $SiCO_3F_2$, $AlNO_3F_2$, PBO_3F_2, and $PB_3O_6F_2$

		λ_{UV} (nm)	d_{ij} (pm/V)	Δn at 400 nm	λ_{PM} (nm)
BCF[#]	calc	147	$d_{11} = 0.87$	0.111	155
$SiCO_3F_2$[#]	calc	129	$d_{16} = 0.96$	0.135	129
$AlNO_3F_2$[#]	calc	173	$d_{16} = 1.63$	0.178	173
PBO_3F_2[#]	calc	135	$d_{16} = 0.61$	0.076	155
$PB_3O_6F_2$[#]	calc	137	$d_{16} = 0.45$	0.099	137

Similar Be-free vdW layered systems can also be designed as shown in Figure 3 (for detailed crystallographic data, see Table S2 in the Supporting Information). Among them, $SiCO_3F_2$ is a typical Be-free DUV NLO carbonate beyond BCF, in which $(SiO_3F_2)^{4-}$ instead of $(BeO_3F)^{5-}$ is connected with planar

DOI: 10.1021/acs.inorgchem.8b01712
Inorg. Chem. 2018, 57, 11146−11156

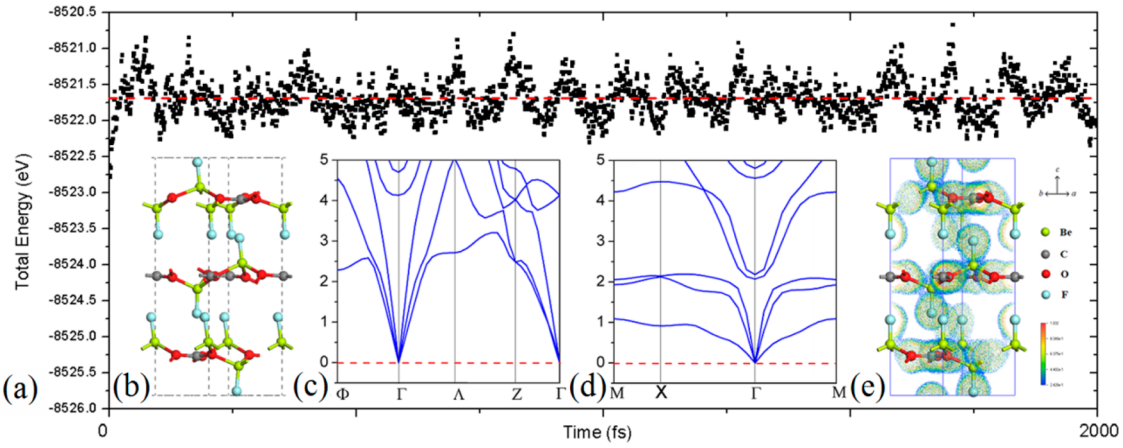

Figure 4. Evolution of total energy (a), structures after a long-time MD simulation (b), phonon spectra of BCF bulk (c) and monolayer (d), and layered electronic density distribution of BCF (e).

$(CO_3)^{4-}$ units by sharing the O atoms to form the AB-stacking polar $(SiCO_3F_2)_\infty$ infinite layers (see Figure 3b). Since silicon has stronger covalence than beryllium, Si-based carbonates can eliminate more nonbonding states of $(CO_3)^{2-}$ than Be-based carbonates, so that $SiCO_3F_2$ actually exhibits a larger energy bandgap ($E_g \approx 9.64$ eV) than BCF (~8.46 eV), and almost the largest so far in all known and designed NLO materials (e.g., BPO_4, $E_g \approx 9.3$ eV).[55] Given the enhancement of SHG effect and birefringence, $SiCO_3F_2$ has the ability to achieve the shorter DUV PM output ($\lambda_{PM} \approx 129$ nm) than BCF (~155 nm), with a theoretically higher conversion efficiency. Note that 129 nm is so far the shortest wavelength for the DUV SHG output. This means that it can achieve the eighth harmonic generation (~133 nm) of the most practical 1064 nm light source of Nd:YAG laser, which has never been realized in the world up to date.

Similar structures can be found in the nitrate and borate system since $(NO_3)^-$ and $(BO_3)^{3-}$ are analogous to $(CO_3)^{2-}$ with similar planar triangle structure with π-conjugated orbitals. On the one hand, $AlNO_3F_2$ is a typical Al-based vdW nitrate with polar $(AlNO_3F_2)_\infty$ layered framework (see Figure 3c). It exhibits a smaller E_g but larger d_{ij} and Δn than BCF and $SiCO_3F_2$, and still can produce a DUV SHG output of 173 nm, which can be considered as a promising NLO material candidate for the practical 193.7 and 177.3 nm lasers. Compared to the common nitrate structures, there is no doubt that $AlNO_3F_2$ exhibits a better (or so far the best) DUV NLO capability. In contrast, none of the nitrate compounds have been shown to exhibit some DUV NLO performances so far. On the other hand, PBO_3F_2 and $PB_3O_6F_2$ are designed to increase the structural anisotropy of BPO_4 by introducing coplanar $(BO_3)^{3-}$ or $(B_3O_6)^{3-}$ units instead of $(BO_4)^{5-}$ (see Figure 3d,e).[55] Simultaneously, fluorine atoms are incorporated into the lattice to form new structural units such as (PO_mF_n), which can further eliminate the nonbonding states and adjust the construction of basic blocks. Compared to BPO_4 (see Table 2), PBO_3F_2 and $PB_3O_6F_2$ exhibit close E_g (~9.2 and 9.1 eV), smaller d_{ij} (~0.61 and 0.45 pm/V), and larger Δn (~0.08 and 0.10), so they can realize DUV PM output of 155 and 137 nm, both shorter than that of KBBF (~161 nm).[67] All results demonstrate that the polar vdW layered structures without A-site cations can facilitate the superior DUV NLO capabilities beyond KBBF.

3.2.3. Practical Capability of the Layered Structures without A-Site Cations. In order to describe the practical capability to produce the DUV laser output, we have to investigate the frequency conversion efficiency, with emphasis on the 6HG of the practical Nd:YAG lasers with wavelength of 1064 nm. Taking BCF as an example, the type-I SHG PM angles can be determined as the fundamental wavelengths of 1100 to 300 nm. The Sellmeier equations obtained by fitting the refractive indices and PM angles are accurate in the UV and DUV regions from 148 to 400 nm (see Figure S5 in the Supporting Information). For the important 177.3 nm SHG output, the PM angle θ for BCF is about 56°, while for KBBF it is about 69°.[4] In the practical type-I PM process (o + o → e), the effective SHG coefficient $d_{eff} = d_{11} \cos\theta \cos 3\psi$, where ψ can be tuned to be zero in the actual situation. As a result, the d_{eff} of BCF is about 3.3 times larger than that of KBBF. Under the non-depletion approximation, the theoretical SHG output power satisfies the following form:

$$P_{2\omega} = \frac{8\pi^2 d_{eff}^2 L^2 I_\omega P_\omega}{\varepsilon_0 n_\omega^2 n_{2\omega} c \lambda_\omega^2}$$

where d_{eff} is the effective SHG coefficient, L the length of a crystal, I_ω the peak power density of the input beam, P_ω the power of the fundamental wave, ε_0 the vacuum permittivity, n_ω and $n_{2\omega}$ the refractive indices at the fundamental λ_ω (354.7 nm) and the second harmonic $\lambda_{2\omega}$ (177.3 nm) along the PM direction, and c the speed of light in a vacuum. According to the formula, one can see that under the same laser input conditions (e.g., P_ω, I_ω, λ_ω) and crystal quality (e.g., L), the output power $P_{2\omega}$ of BCF crystal would be about 10 times larger than that of KBBF. Considering that KBBF device has achieved the applicable DUV output of 177.3 nm with 200 mW power,[9] in principle a similar device based on BCF crystal is capable of generating the DUV 6HG output of practical Nd:YAG 1064 nm laser with a power of about 2 W. Upon being confirmed, it will be the first time to produce a DUV 177.3 nm laser radiation with watt-level power.

In addition, the first-principles MD simulations were performed to confirm that its lattice structure was stable at room temperature. As shown in Figure 4a, the total energy with respect to time oscillates in a corresponding average. Moreover, the structure can be maintained after a long-time MD simulations (~2 ps, see Figure 4b), which indicates that it can be used at room temperature and has a stable structure.

DOI: 10.1021/acs.inorgchem.8b01712
Inorg. Chem. 2018, 57, 11146−11156

Meanwhile, the phonon property is calculated to verify the dynamical stability.[53] The phonon spectrum of BCF bulk in Figure 4c shows that there is not any imaginary phonon mode, which means it is dynamically stable. Besides, the full elastic tensors c_{ij} are determined using the finite strain technique to confirm the Born criterion for a lattice to be stable.[68] From the results of c_{11} = 208.6, c_{33} = 116.1, c_{44} = 47.43, c_{12} = 65.2, c_{13} = 52.2, and c_{14} = −6.3 (unit: GPa), it is easy to verify that the general conditions for stability, $(c_{11} + c_{12})c_{33} - 2c_{13}^2 > 0$ and $(c_{11} - c_{12})c_{44} - 2c_{14}^2 > 0$, are satisfied.[69] Interestingly, no imaginary phonon frequency is found, even in a BCF monolayer (see Figure 4d), indicating that the monolayer of BCF is also structurally stable. Similar to the vdW epitaxial growth of layered structures, numerous BCF monolayers may be formed in the beginning process of crystal growth; as the chemical reaction carries on, adjacent BCF layers are attracted by interlayer vdW interactions, gradually constructing the alternately dense-stacking layered structure. The electronic density of such structure, displayed in Figure 4e, shows that each Be−F upward dipole is embedded with another downward dipole of nearby layer, which actually enhances the interconnection of the whole structure as well as reduces the interlayer slippage within the a−b plane. It should be noted that the dangling F anions of each monolayer are also attracted by the Be^{2+} and C^{4+} cations of the nearby monolayer. Thus, the interlayer Coulomb force would enhance the interlayer connection as well. Table S3 in the Supporting Information lists the distance $r_{\text{atom-atom}}$ and Coulomb force $F_{\text{system},z}$ along the c-axis of the nearest F−Be, F−C, F−F, and F−O between layers of BCF as well as those of KBBF. From the approximate calculations, it is estimated that the $F_{\text{BCF},z}$ of BCF is about 3.58 times $F_{\text{KBBF},z}$ of KBBF along the c-axis:

$$\frac{F_{\text{BCF},z}}{F_{\text{KBBF},z}} \approx \left(\sum_{\langle i,j\rangle} n_{ij}\frac{q_i q_j}{r_{ij}^3} r_{ij,z}\right)_{\text{BCF}} \Bigg/ \left(\sum_{\langle i,j\rangle} n_{ij}\frac{q_i q_j}{r_{ij}^3} r_{ij,z}\right)_{\text{KBBF}} = 3.58$$

The above analysis clearly demonstrates that BCF crystal exhibits stronger interlayer interaction than KBBF crystal along the c-axis, which means that the BCF crystal is more feasible to grow in a large-scale sample than KBBF especially along the crystal c-axis. In addition, from the calculated mechanical and thermal properties (for details see the analysis in Table S4 in the Supporting Information), BCF is predicted to exhibit more favorable performances of machining and heat resistance than KBBF, which are very important for high-intensity laser applications.

For other layered structures without A-site cations, such as $AlCO_3F$, YCO_3F, $SiBO_3F$, SiB_3O_6F, $SiCO_3F_2$, $AlNO_3F_2$, PBO_3F_2 and $PB_3O_6F_2$, we also calculated the phonon spectra to verify their dynamical stabilities as shown in Figure S6 in the Supporting Information. Among them, only $AlCO_3F$, $SiCO_3F_2$, $AlNO_3F_2$, PBO_3F_2, and $PB_3O_6F_2$ are dynamically stable without any virtual frequency, whereas the other three exhibit some structural instability. In addition, Pauling's rules are usually adopted to investigate the structural reasonability and stability for the ionic compounds, although some might be violated under extreme conditions.[70] According to Pauling's second rule, the bond valence sum (BVS) of O^{2-} anions should be generally in a reasonable region from 1.75 to 2.25 (2 is the best) to guarantee the structural stability. From the simple estimation, the BVS of the bridged O^{2-} in $AlCO_3F$, $SiCO_3F_2$, $AlNO_3F_2$, PBO_3F_2, and $PB_3O_6F_2$ are 1.9, 2.13, 2.27, 2.0 and 2.0, respectively. Note that among the known compounds,[71,72] e.g., in $Cs_2Al(NO_3)_5$ (or $Co_3BP_3O_{14}$), NO_3 (or BO_3) is corner-shared by AlO_6 (or PO_4), corresponding to the BCS about 2.17 (or 2.25). Therefore, the BVS results of the above five compounds are acceptable in some degree although they maybe not the most stable phases. In fact, there are also some other structures with similar layered structural features but different symmetries according to the proposed design strategy. For example, we can design another phase of PBO_3F_2 and $PB_3O_6F_2$ with ABC stacking of $R3$ space group instead of those with AB stacking of $P\bar{6}2c$. For comparison, these phases of PBO_3F_2 and $PB_3O_6F_2$ exhibit higher total energies but close DUV NLO capabilities including energy bandgaps, SHG effects, birefringence and the PM outputs from the same calculations (see Table S5 in the Supporting Information). No matter which structural phases can be obtained from the experiments, we have already provided the strategy to design the NLO structures with better DUV PM SHG capability, which will facilitate the search for new DUV NLO materials with enhanced DUV NLO capabilities especially in the layered framework system without A-site cations.

3.2.4. Evaluation for Possible Applications. We will now present a perspective on the output capabilities of DUV lasers and possible applications of the proposed structures without A-site cations, especially for those experimentally promising materials including BCF, $AlCO_3F$, $AlNO_3F$, PBO_3F_2, $PB_3O_6F_2$, and $SiCO_3F_2$. Above all, Figure 5 depicts the coordinates of the

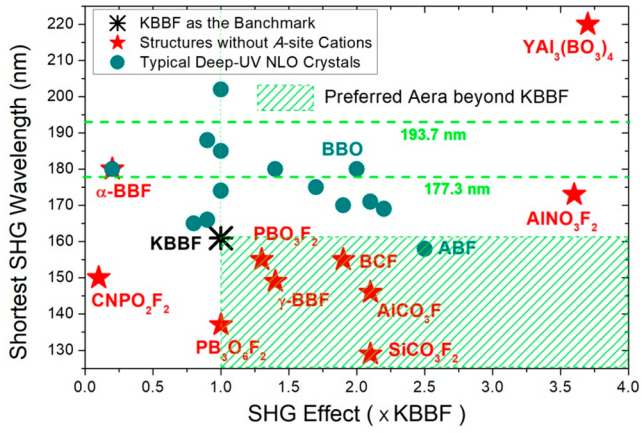

Figure 5. DUV NLO coordinates of typical known and designed materials. The green shadow is the preferred area of DUV NLO materials beyond KBBF.

SHG effects and shortest SHG output wavelengths for most of the available DUV NLO compounds, with reference marks of 193.7 and 177.3 nm for the two actual laser sources. Note that KBBF is labeled as a black star as the benchmark DUV NLO material with d_{16} = 0.45 pm/V and λ_{PM} = 161 nm. Circular dots are those typical and conventional DUV NLO structures with A-site cations. From left to right, $BaBe_2BO_3F_3$,[40] RbB_4O_6F,[73] NaB_4O_6F,[74] ABBF, NBBF, RBBF, $BaB_4O_6F_2$,[75] CsB_4O_6F,[73] $CsKB_8O_{12}F_2$,[73] β-BaB_2O_4 (BBO),[76] $Ca_2B_{10}O_{14}F_6$,[37] $Sr_2B_{10}O_{14}F_6$,[37] and $NH_4B_4O_6F$ (ABF)[36] exhibit the ability to achieve the SHG PM output below 193.7 nm, although $BaBe_2BO_3F_3$, ABBF, NBBF, and $BaB_4O_6F_2$ are not as good as BBO, which is a famous NLO material still unavailable

DOI: 10.1021/acs.inorgchem.8b01712
Inorg. Chem. 2018, 57, 11146−11156

for the DUV SHG generation. Among them, $Ca_2B_{10}O_{14}F_6$, $Sr_2B_{10}O_{14}F_6$, $CsKB_8O_{12}F_2$ and ABF exhibit a stronger SHG effect than KBBF and RBBF, so that theoretically they can be used as promising DUV NLO materials for 6HG 177.3 nm output with higher conversion efficiency. When it comes to our proposed structures without A-site cations (marked by the red pentagrams), it should be noted that $CNPO_2F_2$ can output a shorter PM wavelength than those of circular dots although its SHG effect is too small, and $AlNO_3F_2$ can exhibit the largest SHG effect (~3.7 × KBBF) in all of the DUV NLO structures with effective $\lambda_{PM} \approx 173$ nm < 177.3 nm. More importantly, the preferred region of the NLO materials with better DUV capabilities beyond KBBF is further highlighted with shorter λ_{PM} (<161 nm) and larger $|d_{ij}|_{max}$ (>KBBF) in the green shadow area of Figure 5. It is worth noting that only one circular point (i.e., ABF) is found to be located in this area, whereas six red pentagrams (i.e., $PB_3O_6F_2$, PBO_3F_2, γ-BBF, BCF, $AlCO_3F$, and $SiCO_3F_2$) are predicted to exhibit more excellent DUV output capabilities than KBBF. Based on the proposed design strategy, the probability of the available DUV NLO crystals beyond KBBF is so high, fully indicating that the polar layered structures without A-site cations are more favorable as the promising DUV NLO candidates to replace the KBBF.

Importantly, similar to KBBF, the proposed $AlNO_3F_2$, $PB_3O_6F_2$, PBO_3F_2, γ-BBF, BCF, $AlCO_3F$, and $SiCO_3F_2$ can be used as the NLO devices for the DUV laser output of 193.7 and 177.3 nm, which have several important applications in super-high-resolution photoemission spectrograph, photoemission electron microscopy, and 193 nm photolithography.[7,9] Moreover, all of them can achieve a theoretically higher NLO conversion efficiency than KBBF due to the larger PM SHG effects. Therefore, the crystal is expected to realize the DUV laser output with watt-level power. $PB_3O_6F_2$ and $SiCO_3F_2$, once obtained in the experiments, would offer possible applications that cannot be realized by KBBF. For example, both of them can achieve the fifth harmonic generation output (138.9 nm) of ruby laser, and tunable DUV generation from 137/129 to 200 nm using a Ti-sapphire laser. Remarkably, $SiCO_3F_2$ could be applied to realize the eighth harmonic generation (~133 nm) of the most practical Nd:YAG laser source, which is the only material that could achieve this application until now. All of the achievements demonstrate that they can provide more powerful laser resources for materials science and technology. In addition, since $AlNO_3F_2$, $PB_3O_6F_2$, PBO_3F_2, BCF, and $SiCO_3F_2$ are vdW crystals with dynamically stable monolayers, they can also be further cleaved as 2D materials. Computational analysis shows that these monolayers can well maintain the DUV NLO capabilities of the corresponding crystals while having strong SHG effects and wide transparent windows. Therefore, they might be applied in some optical film devices with available NLO or photoelastic effects.[77,78]

4. OUTLOOK AND CONCLUSION

One of the most important issues in the field of laser technology is the realization of practical DUV laser output with short wavelength and high power. NLO crystals are considered to be the key components of all-solid-state lasers, a very important way to generate DUV coherent light by frequency conversion. The field of DUV NLO materials has been rapidly developed for decades, but there are still very few commercially available DUV laser sources with high output power and good conversion efficiency. As the only current practical DUV NLO crystal, KBBF exhibits the extreme difficulty of growing large-size crystals and relatively small SHG effect. This allows it to achieve the practical 177.3 nm laser output with 200 mW power so far, but that is still below watt level. In order to find new DUV NLO materials beyond KBBF, theoretical modeling and simulations have become an effective and efficient technique for current research. In view of the difficulty in finding known compounds that meet the requirements of DUV NLO materials, modeling new rational structures based on computer-aided methods can provide more insight into the experimental probes. More importantly, the computational methods developed are accurate, allowing us to better understand the structure−property relations of DUV NLO crystals.

Therefore, in this article, we provided a systematic overview of the DUV NLO effect induced by the A-site alkali and alkaline earth metal cations. Accordingly, we have found a strategy for designing new DUV NLO materials through bridge-bonded and vdW-connected dense-stacking without A-site cations, which is quite different from the previous design strategies. Many attempts have been made but failed to break the limit of KBBF due to the lack of such a strategy. Based on the new findings, we have used state-of-the-art methods to evaluate the DUV NLO capabilities of many known and designed structures without A-site cations. Remarkably, many proposed structures can exhibit excellent DUV NLO capabilities with wide energy bandgaps, strong SHG effects, and large birefringence in the DUV region. For example, a novel vdW lattice of BCF is predicted to be an alternative DUV NLO material, beyond KBBF, because it can achieve shorter PM SHG output and higher conversion efficiency than KBBF. Moreover, BCF can exhibit good structural stability and more favorable performances of growth ability, machining, and heat resistance, which are important for high-intensity laser applications. It is therefore capable of generating practical 6HG output (177.3 nm) from a Nd:YAG laser with watt-level power, which is of great value to provide more powerful tools for physics and materials science and has not yet been realized. In addition to BCF, several other structures (e.g., $AlNO_3F_2$, $PB_3O_6F_2$, PBO_3F_2, $AlCO_3F$, and $SiCO_3F_2$) are also predicted as promising DUV NLO materials with better capabilities than KBBF. Meanwhile, their structures are theoretically stable and thus possible to be synthesized like γ-BBF in suitable experiments. Once obtained, some of them (e.g., $PB_3O_6F_2$ and $SiCO_3F_2$) would be able to realize some new optical applications, e.g., eighth harmonic generation output (133 nm) of Nd:YAG laser. Note that (1) $AlNO_3F_2$ exhibits so far the largest SHG effect (3.7 × KBBF) in the DUV region, so it can achieve the 177.3 nm laser output with much higher output power, over watt-level, and (2) $SiCO_3F_2$ can output so far the shortest DUV SHG wavelength (~129 nm), so it fills the gap of DUV all-solid-state lasers between 100 and 140 nm. All of the results clearly demonstrate that the structures with and without the A-site cations are essentially different in their abilities to achieve the DUV NLO capability.[76−78]

In conclusion, we have revealed a breakthrough strategy to design new NLO crystals beyond KBBF for an enhanced DUV NLO capability through layered dense-stacking connection without A-site cations. The key point in our attempt to communicate with experimentalists is that, if the A-site alkali and alkaline earth metal cations can be removed in the experimental synthesis, the resulting layered structures will be

DOI: 10.1021/acs.inorgchem.8b01712
Inorg. Chem. 2018, 57, 11146−11156

very beneficial for enhancing the DUV PM and frequency conversion capability. Accordingly, two series of polar layered framework structures, i.e., (i) F-bridge-bonded γ-BBF and $AlCO_3F$ and (ii) vdW-connected BCF, $AlNO_3F_2$, $PB_3O_6F_2$, PBO_3F_2, and $SiCO_3F_2$, are predicted as very competitive candidates to replace KBBF based on their excellent DUV NLO capabilities. In particular, they are promising to be used to produce 6HG output (177.3 nm) of a Nd:YAG laser with higher power and to make a more powerful DUV laser with shorter wavelengths. Of course, these achievements are the first step which indicate that there are indeed some better DUV NLO materials than KBBF that are structurally stable and theoretically possible to be obtained in practice. The second step will be to synthesize those compounds in suitable experiments, as in the case of γ-BBF.[35] Further, crystal growth with large material size and high optical quality is necessary for practical applications. Note that more attempts for crystal growth are worthwhile only when more theoretically promising compounds are obtained. Under the guidance of the proposed strategy, several DUV NLO compounds are designed theoretically in this work—more than ever before—which leads us to believe that the prospects for exploration of promising new DUV NLO materials beyond KBBF are optimistic.

■ ASSOCIATED CONTENT

Supporting Information

The Supporting Information is available free of charge on the ACS Publications website at DOI: 10.1021/acs.inorgchem.8b01712.

Computational methods, including Tables S1−S5 and Figures S1−S6: crystal structures of $MBe_2BO_3F_2$ (M = K, Rb, Cs, Tl), NBBF, and ABBF; crystallographic data of typical KBBF-family crystals; interlayer distance, cationic size, and volume per formula unit with respect to the ionic radius in the KBBF-family crystals; PDOS analysis of TBBF; crystal structures of BPO_4, $CNPO_2F_2$, $YAl_3(BO_3)_4$, and YCO_3OH; calculated crystallographic data of designed YCO_3F, $AlCO_3F$, $SiBO_3F$, SiB_3O_6F, $Be_2CO_3F_2$, $SiCO_3F_2$, $AlNO_3F_2$, PBO_3F_2, and $PB_3O_6F_2$; type-I phase-matching angles with respect to fundamental wavelength for BCF; interlayer interaction data for BCF and KBBF; calculated mechanical and thermal properties of BCF and KBBF; calculated phonon spectra of $AlCO_3F$, $SiCO_3F_2$, $AlNO_3F_2$, PBO_3F_2, and $PB_3O_6F_2$; and calculated crystallographic data and NLO properties of new phases of PBO_3F_2 and $PB_3O_6F_2$ (PDF)

■ AUTHOR INFORMATION

Corresponding Authors

*E-mail: zslin@mail.ipc.ac.cn.
*E-mail: fliu@eng.utah.edu.
*E-mail: bing.huang@csrc.ac.cn.

ORCID

Lei Kang: 0000-0002-9993-6399
Zheshuai Lin: 0000-0002-9829-9893
Feng Liu: 0000-0002-3701-8058

Notes

The authors declare no competing financial interest.

■ ACKNOWLEDGMENTS

This work was supported by NSFC Grants Nos. 11574024, 91622118, 11704023 and NSAF U1530401. F.L. acknowledges support from the U.S. DOE-BES (No. DE-FG02-04ER46148). Z.L. acknowledges support from the Outstanding Member in Youth Innovation Promotion Association at CAS.

■ REFERENCES

(1) Jones-Bey, H. Deep-UV Applications Await Improved Nonlinear Optics. *Laser Focus World* **1998**, *34*, 127.
(2) Togashi, T.; Nabekawa, N.; Sekikawa, T.; Watanabe, S. Generation of Milliwatt Narrow-Bandwidth Vacuum Ultraviolet Radiation by An All-Solid-State Tunable High-Average-Power Laser System. *Opt. Lett.* **2001**, *26*, 831−833.
(3) Xia, Y. N.; Chen, C. T.; Tang, D. Y.; Wu, B. C. New Nonlinear-Optical Crystals for UV and VUV Harmonic-Generation. *Adv. Mater.* **1995**, *7*, 79−81.
(4) Chen, C. T.; Ye, N.; Lin, J.; Jiang, J.; Zeng, W. R.; Wu, B. C. Computer-Assisted Search for Nonlinear Optical Crystals. *Adv. Mater.* **1999**, *11*, 1071−1078.
(5) Chen, C.; Lin, Z.; Wang, Z. Deep-UV Nonlinear Optical Crystal $KBe_2BO_3F_2$-Discovery, Growth, Optical Properties and Applications. *Appl. Phys. B: Lasers Opt.* **2005**, *80*, 1−25.
(6) Tran, T. T.; Yu, H. W.; Rondinelli, J. M.; Poeppelmeier, K. R.; Halasyamani, P. S. Deep Ultraviolet Nonlinear Optical Materials. *Chem. Mater.* **2016**, *28*, 5238−5258.
(7) Chen, C. T.; Wang, G. L.; Wang, X. Y.; Xu, Z. Y. Deep-UV Nonlinear Optical Crystal $KBe_2BO_3F_2$-Discovery, Growth, Optical Properties and Applications. *Appl. Phys. B: Lasers Opt.* **2009**, *97*, 9−25.
(8) Chen, C. T.; Wang, Y. B.; Wu, B. C.; Wu, K. C.; Zeng, W. L.; Yu, L. H. Design and Synthesis of an Ultraviolet-Transparent Nonlinear-Optical Crystal $Sr_2Be_2B_2O_7$. *Nature* **1995**, *373*, 322−324.
(9) Xu, B.; Liu, L. J.; Wang, X. Y.; Chen, C. T.; Zhang, X.; Lin, S. J. Generation Of High Power 200 MW Laser Radiation at 177.3 nm in $KBe_2BO_3F_2$ Crystal. *Appl. Phys. B: Lasers Opt.* **2015**, *121*, 489−494.
(10) Chen, C. T.; Luo, S. Y.; Wang, X. Y.; Wang, G. L.; Wen, X. H.; Wu, H. X.; Zhang, X.; Xu, Z. Y. Deep UV Nonlinear Optical Crystal: $RbBe_2(BO_3)F_2$. *J. Opt. Soc. Am. B* **2009**, *26*, 1519−1525.
(11) Huang, H. W.; Chen, C. T.; Wang, X. Y.; Zhu, Y.; Wang, G. L.; Zhang, X.; Wang, L. R.; Yao, J. Y. Deep UV Nonlinear Optical Crystal: $CsBe_2(BO_3)F_2$. *J. Opt. Soc. Am. B* **2011**, *28*, 2186−2190.
(12) Hu, Z. G.; Yoshimura, M.; Muramatsu, K.; Mori, Y.; Sasaki, T. A New Nonlinear Optical Crystal $BaAlBO_3F_2$ (BABF). *Jpn. J. Appl. Phys. Part 2 - Lett.* **2002**, *41*, L1131−L1133.
(13) Li, R. K.; Chen, P. Cation Coordination Control of Anionic Group Alignment to Maximize SHG Effects in the $BaMBO_3F$ (M = Zn, Mg) Series. *Inorg. Chem.* **2010**, *49*, 1561−1565.
(14) Wang, S. C.; Ye, N.; Li, W.; Zhao, D. Alkaline Beryllium Borate $NaBeB_3O_6$ and $ABe_2B_3O_7$ (A = K, Rb) as UV Nonlinear Optical Crystals. *J. Am. Chem. Soc.* **2010**, *132*, 8779−8786.
(15) Wu, H. P.; Pan, S. L.; Poeppelmeier, K. R.; Li, H. Y.; Jia, D. Z.; Chen, Z. H.; Fan, X. Y.; Yang, Y.; Rondinelli, J. M.; Luo, H. S. $K_3B_6O_{10}Cl$: A New Structure Analogous to Perovskite with a Large Second Harmonic Generation Response and Deep UV Absorption Edge. *J. Am. Chem. Soc.* **2011**, *133*, 7786−7790.
(16) Huang, H. W.; Yao, J. Y.; Lin, Z. S.; Wang, X. Y.; He, R.; Yao, W. J.; Zhai, N. X.; Chen, C. T. $NaSr_3Be_3B_3O_9F_4$: A Promising Deep-Ultraviolet Nonlinear Optical Material Resulting From the Cooperative Alignment of the $Be_3B_3O_{12}F^{10-}$ Anionic Group. *Angew. Chem., Int. Ed.* **2011**, *50*, 9141−9144.
(17) Wang, S. C.; Ye, N. $Na_2CsBe_6B_5O_{15}$: An Alkaline Beryllium Borate as a Deep-UV Nonlinear Optical Crystal. *J. Am. Chem. Soc.* **2011**, *133*, 11458−11461.
(18) Huang, H. W.; Yao, J. Y.; Lin, Z.; Wang, X. Y.; He, R.; Yao, W. J.; Zhai, N. X.; Chen, C. T. Molecular Engineering Design To Resolve the Layering Habit and Polymorphism Problems in Deep UV NLO

DOI: 10.1021/acs.inorgchem.8b01712
Inorg. Chem. 2018, 57, 11146−11156

Crystals: New Structures In MM'$Be_2B_2O_6F$ (M = Na, M'=Ca; M= K, M'=Ca, Sr). *Chem. Mater.* **2011**, *23*, 5457−5463.
(19) Yu, H. W.; Wu, H. P.; Pan, S. L.; Yang, Z. H.; Su, X.; Zhang, F. F. A Novel Deep UV Nonlinear Optical Crystal $Ba_3B_6O_{11}F_2$, with a New Fundamental Building Block, B_6O_{14} Group. *J. Mater. Chem.* **2012**, *22*, 9665−9670.
(20) Wu, H. P.; Yu, H. W.; Yang, Z. H.; Hou, X. L.; Su, X.; Pan, S. L.; Poeppelmeier, K. R.; Rondinelli, J. M. Designing A Deep-Ultraviolet Nonlinear Optical Material with A Large Second Harmonic Generation Response. *J. Am. Chem. Soc.* **2013**, *135*, 4215−4218.
(21) Yan, X.; Luo, S. Y.; Lin, Z. S.; Yao, J. Y.; He, R.; Yue, Y. C.; Chen, C. T. $ReBe_2B_5O_{11}$ (Re = Y, Gd): Rare-Earth Beryllium Borates as Deep-Ultraviolet Nonlinear-Optical Materials. *Inorg. Chem.* **2014**, *53*, 1952−1954.
(22) Zhao, S. G.; Gong, P. F.; Bai, L.; Xu, X.; Zhang, S. Q.; Sun, Z. H.; Lin, Z. S.; Hong, M. C.; Chen, C. T.; Luo, J. H. Beryllium-Free $Li_4Sr(BO_3)_2$ for Deep-Ultraviolet Nonlinear Optical Applications. *Nat. Commun.* **2014**, *5*, 4019.
(23) Zhao, S. G.; Gong, P. F.; Luo, S. Y.; Liu, S. J.; Li, L. N.; Asghar, M. A.; Khan, T.; Hong, M. C.; Lin, Z. S.; Luo, J. H. Beryllium-Free $Rb_3Al_3B_3O_{10}F$ with Reinforced Inter Layer Bonding as A Deep-Ultraviolet Nonlinear Optical Crystal. *J. Am. Chem. Soc.* **2015**, *137*, 2207−2210.
(24) Tran, T. T.; Koocher, N. Z.; Rondinelli, J. M.; Halasyamani, P. S. Beryllium-Free Beta-$Rb_2Al_2B_2O_7$ as A Possible Deep-Ultraviolet Nonlinear Optical Material Replacement for $KBe_2BO_3F_2$. *Angew. Chem., Int. Ed.* **2017**, *56*, 2969−2973.
(25) Zhang, B. B.; Shi, G. Q.; Yang, Z. H.; Zhang, F. F.; Pan, S. L. Fluorooxoborates: Beryllium-Free Deep-Ultraviolet Nonlinear Optical Materials without Layered Growth. *Angew. Chem., Int. Ed.* **2017**, *56*, 3916−3919.
(26) Zou, G. H.; Ye, N.; Huang, L.; Lin, X. S. Alkaline-Alkaline Earth Fluoride Carbonate Crystals $ABCO_3F$ (A = K, Rb, Cs; B = Ca, Sr, Ba) as Nonlinear Optical Materials. *J. Am. Chem. Soc.* **2011**, *133*, 20001−20007.
(27) Tran, T. T.; He, J. G.; Rondinelli, J. M.; Halasyamani, P. S. $RbMgCO_3F$: A New Beryllium-Free Deep-Ultraviolet Nonlinear Optical Material. *J. Am. Chem. Soc.* **2015**, *137*, 10504−10507.
(28) Yu, P.; Wu, L. M.; Zhou, L. J.; Chen, L. Deep-Ultraviolet Nonlinear Optical Crystals: $Ba_3P_3O_{10}X$ (X = Cl, Br). *J. Am. Chem. Soc.* **2014**, *136*, 480−487.
(29) Zhao, S. G.; Gong, P. F.; Luo, S. Y.; Bai, L.; Lin, Z. S.; Ji, C. M.; Chen, T. L.; Hong, M. C.; Luo, J. H. Deep-Ultraviolet Transparent Phosphates $RbBa_2(PO_3)_5$ and $Rb_2Ba_3(P_2O_7)_2$ Show Nonlinear Optical Activity From Condensation Of PO_4^{3-} Units. *J. Am. Chem. Soc.* **2014**, *136*, 8560−8563.
(30) Zhao, S. G.; Gong, P. F.; Luo, S. Y.; Bai, L.; Lin, Z. S.; Tang, Y. Y.; Zhou, Y. L.; Hong, M. C.; Luo, J. H. Tailored Synthesis Of A Nonlinear Optical Phosphate with A Short Absorption Edge. *Angew. Chem., Int. Ed.* **2015**, *54*, 4217−4221.
(31) Yu, H. W.; Zhang, W. G.; Young, J.; Rondinelli, J. M.; Halasyamani, P. S. Design and Synthesis of the Beryllium-Free Deep-Ultraviolet Nonlinear Optical Material $Ba_3(ZnB_5O_{10})PO_4$. *Adv. Mater.* **2015**, *27*, 7380−7385.
(32) Kang, L.; Luo, S. Y.; Huang, H. W.; Ye, N.; Lin, Z. S.; Qin, J. G.; Chen, C. T. Prospects for Fluoride Carbonate Nonlinear Optical Crystals in the UV and Deep-UV Regions. *J. Phys. Chem. C* **2013**, *117*, 25684−25692.
(33) Kang, L.; Lin, Z. S.; Qin, J. G.; Chen, C. T. Two Novel Nonlinear Optical Carbonates in the Deep-Ultraviolet Region: $KBeCO_3F$ and $RbAlCO_3F_2$. *Sci. Rep.* **2013**, *3*, 1366.
(34) Kang, L.; Luo, S. Y.; Peng, G.; Ye, N.; Wu, Y. C.; Chen, C. T.; Lin, Z. S. First-Principles Design of A Deep-Ultraviolet Nonlinear-Optical Crystal From $KBe_2BO_3F_2$ to $NH_4Be_2BO_3F_2$. *Inorg. Chem.* **2015**, *54*, 10533−10535.
(35) Peng, G.; Ye, N.; Lin, Z. S.; Kang, L.; Pan, S.; Zhang, M.; Lin, C.; Long, X. F.; Luo, M.; Chen, Y.; Tang, Y.; Xu, F.; Yan, T. $NH_4Be_2BO_3F_2$ and γ-$Be2BO_3F$: Overcoming the Layering Habit in $KBe_2BO_3F_2$ for the Next Generation Deep-Ultraviolet Nonlinear Optical Materials. *Angew. Chem.* **2018**, *130*, 9106.
(36) Shi, G. Q.; Wang, Y.; Zhan, F. F.; Zhang, B. B.; Yang, R. H.; Hou, X. L.; Pan, S. L.; Poeppelmeier, K. R. Finding the Next Deep-Ultraviolet Nonlinear Optical Material: $NH_4B_4O_6F$. *J. Am. Chem. Soc.* **2017**, *139*, 10645−10648.
(37) Luo, M.; Liang, F.; Song, Y.; Zhao, D.; Xu, F.; Ye, N.; Lin, Z. $M_2B_{10}O_{14}F_6$ (M = Ca, Sr): Two Noncentrosymmetric Alkaline Earth Fluorooxoborates as Promising Next-Generation Deep-Ultraviolet Nonlinear Optical Materials. *J. Am. Chem. Soc.* **2018**, *140*, 3884−3887.
(38) Kang, L.; Luo, S. Y.; Huang, H. W.; Zheng, T.; Lin, Z. S.; Chen, C. T. Ab Initio Studies on the Optical Effects in the Deep Ultraviolet Nonlinear Optical Crystals of the $KBe_2BO_3F_2$ Family. *J. Phys.: Condens. Matter* **2012**, *24*, 335503.
(39) Mei, L. F.; Wang, Y. B.; Chen, C. T.; Wu, B. C. Nonlinear-Optical Materials Based on $MBe_2BO_3F_2$ (M = Na, K). *J. Appl. Phys.* **1993**, *74*, 7014−7015.
(40) Guo, S.; Jiang, X. X.; Liu, L. J.; Xia, M. J.; Fang, Z.; Wang, X. Y.; Lin, Z. S.; Chen, C. T. $BaBe_2BO_3F_3$: A KBBF-Type Deep-Ultraviolet Nonlinear Optical Material with Reinforced $Be2BO_3F_2$ (Infinity) Layers and Short Phase-Matching Wavelength. *Chem. Mater.* **2016**, *28*, 8871−8875.
(41) Yao, W. J.; He, R.; Wang, X. Y.; Lin, Z. S.; Chen, C. T. Analysis of Deep-UV Nonlinear Optical Borates: Approaching The End. *Adv. Opt. Mater.* **2014**, *2*, 411−417.
(42) Lin, J.; Lee, M. H.; Liu, Z. P.; Chen, C. T.; Pickard, C. J. Mechanism for Linear and Nonlinear Optical Effects in Beta-BaB_2O_4 Crystals. *Phys. Rev. B: Condens. Matter Mater. Phys.* **1999**, *60*, 13380−13389.
(43) Lin, Z. S.; Jiang, X. X.; Kang, L.; Gong, P. F.; Luo, S. Y.; Lee, M. H. First-Principles Materials Applications and Design of Nonlinear Optical Crystals. *J. Phys. D: Appl. Phys.* **2014**, *47*, 253001.
(44) Payne, M. C.; Teter, M. P.; Allan, D. C.; Arias, T. A.; Joannopoulos, J. D. Iterative Minimization Techniques for Abinitio Total-Energy Calculations - Molecular-Dynamics and Conjugate Gradients. *Rev. Mod. Phys.* **1992**, *64*, 1045−1097.
(45) Clark, S. J.; Segall, M. D.; Pickard, C. J.; Hasnip, P. J.; Probert, M. J.; Refson, K.; Payne, M. C. First Principles Methods Using CASTEP. *Z. Kristallogr. - Cryst. Mater.* **2005**, *220*, 567−570.
(46) Rappe, A. M.; Rabe, K. M.; Kaxiras, E.; Joannopoulos, J. D. Optimized Pseudopotentials. *Phys. Rev. B: Condens. Matter Mater. Phys.* **1990**, *41*, 1227−1230.
(47) Monkhorst, H. J.; Pack, J. D. Special Points for Brillouin-Zone Integrations. *Phys. Rev. B* **1976**, *13*, 5188−5192.
(48) Pfrommer, B. G.; Cote, M.; Louie, S. G.; Cohen, M. L. Relaxation of Crystals with the Quasi-Newton Method. *J. Comput. Phys.* **1997**, *131*, 233−240.
(49) Adamo, C.; Barone, V. Toward Reliable Density Functional Methods without Adjustable Parameters: the PBE0Model. *J. Chem. Phys.* **1999**, *110*, 6158−6170.
(50) Perdew, J. P.; Burke, K.; Ernzerhof, M. Generalized Gradient Approximation Made Simple. *Phys. Rev. Lett.* **1996**, *77*, 3865−3868.
(51) Lin, Z. S.; Kang, L.; Zheng, T.; He, R.; Huang, H.; Chen, C. T. Strategy for the Optical Property Studies in Ultraviolet Nonlinear Optical Crystals from Density Functional Theory. *Comput. Mater. Sci.* **2012**, *60*, 99−104.
(52) Baroni, S.; de Gironcoli, S.; Dal Corso, A.; Giannozzi, P. Phonons and Related Crystal Properties from Density-Functional Perturbation Theory. *Rev. Mod. Phys.* **2001**, *73*, 515−562.
(53) Yao, Y.; Tse, J. S.; Sun, J.; Klug, D. D.; Martonak, R.; Iitaka, T. Comment on "New Metallic Carbon Crystal". *Phys. Rev. Lett.* **2009**, *102*, 9601.
(54) McMillen, C. D.; Hu, J.; VanDerveer, D.; Kolis, J. W. Trigonal Structures of $ABe_2BO_3F_2$ (A = Rb, Cs, Tl) Crystals. *Acta Crystallogr., Sect. B: Struct. Sci.* **2009**, *65*, 445−449.
(55) Li, Z. H.; Lin, Z. H.; Wu, Y. C.; Fu, P. Z.; Wang, Z. Z.; Chen, C. T. Crystal Growth, Optical Properties Measurement, and Theoretical Calculation of BPO_4. *Chem. Mater.* **2004**, *16*, 2906−2908.

DOI: 10.1021/acs.inorgchem.8b01712
Inorg. Chem. 2018, 57, 11146−11156

(56) Poojary, D. M.; Borade, R. B.; Cambell, F. L.; Clearfield, A. Crystal Structure of Silicon Pyrophosphate (Form I) from Powder Diffraction Data. *J. Solid State Chem.* **1994**, *112*, 106−112.
(57) Rankin, D. W. H.; Blake, A.; Davis, M.; Ebsworth, E.; Welch, A. The Structure of $PO(OPF_2)_3$ in the Gaseous and Crystalline Phases. *J. Chem. Soc., Dalton Trans.* **1989**, 223−228.
(58) Graia, M.; Driss, A. $Y_2SiP_4O_{15}$. *J. Soc. Alger. Chim.* **2009**, *19*, 27−36.
(59) Kuz'micheva, G. M.; Rybakov, V. B.; Kutovoi, S. A.; Panyutin, V. L.; Oleinik, A. Y.; Plashkarev, O. G. Preparation, Structure, and Properties of New Laser Crystal $Y_2SiBe_2O_7$ and $Y_2AlBeBO_7$. *Inorg. Mater.* **2002**, *38*, 60−65.
(60) Sokolova, E. V.; Azizov, A. V.; Simonov, N. A.; Leonjuk, N. I.; Belov, N. V. The Crystal Structure of the Synthetic Ortho-Tri-Borate $Al_5(BO_3)O_6$. *Dok. Akad. Nauk SSSR* **1978**, *243*, 655−658.
(61) Schultz, E.; Liebau, F. Crystal Structure of Beryllium Phosphate BeP_2O_6 III - A Derivate of Silica K (Keatite). *Z. Kristallogr. - Cryst. Mater.* **1981**, *154*, 115−126.
(62) Yu, X. S.; Yue, Y. C.; Yao, J. Y.; Hu, Z. G. $YAl_3(BO_3)_4$: Crystal Growth and Characterization. *J. Cryst. Growth* **2010**, *312*, 3029−3033.
(63) Beall, G. W.; Milligan, W. O.; Mroczkowski, S. Yttrium Carbonate Hydroxide. *Acta Crystallogr., Sect. B: Struct. Crystallogr. Cryst. Chem.* **1976**, *B32*, 3143−3144.
(64) Zeng, X.; Gerken, M.; Beckers, H.; Willner, H. Spectroscopic and Structural Studies of Difluorophosphoryl azide $F_2P(O)N_3$, Difluorophosphoryl Isocyanate $F_2P(O)NCO$, and Difluorophosphoric Acid Anhydride, $F_2(O)POP(O)F_2$. *Inorg. Chem.* **2010**, *49*, 3002−3010.
(65) Xia, M.; Lin, Z.; Wu, Y.; Chen, C. A New Type of Potential Nonlinear Optical Material-Beryllium Fluoride Borate. *J. Synth. Cryst.* **2005**, *34*, 597−598.
(66) Bian, Q.; Yang, Z.; Wang, Y.; Mutailipu, M.; Ma, Y.; Pan, S. Computer-Assisted Design of a Superior Be_2BO_3F Deep-Ultraviolet Nonlinear-Optical Material. *Inorg. Chem.* **2018**, *57*, 5716.
(67) Kang, L.; Liang, F.; Gong, P.; Lin, Z.; Liu, F.; Huang, B. Two Novel Deep-Ultraviolet Nonlinear Optical Crystals with Shorter Phase-Matching Second Harmonic Generation than $KBe_2BO_3F_2$: A First-Principles Prediction. *Phys. Status Solidi RRL* **2018**, 1800276.
(68) Karki, B. B.; Ackland, G. J.; Crain, J. Elastic Instabilities in Crystals from Ab Initio Stress-Strain Relations. *J. Phys.: Condens. Matter* **1997**, *9*, 8579−8589.
(69) Cowley, R. A. Acoustic Phonon Instabilities and Structural Phase-Transitions. *Phys. Rev. B* **1976**, *13*, 4877−4885.
(70) Huppertz, H.; von der Eltz, B. Multianvil High-Pressure Synthesis of $Dy_4B_6O_{15}$: The First Oxoborate with Edge-Sharing BO_4 Tetrahedra. *J. Am. Chem. Soc.* **2002**, *124*, 9376−9377.
(71) D'yachenko, O. A.; Atovmyan, L. O. Molecular and Crystal Structure of Cesium Pentanitratoaluminate. *J. Struct. Chem.* **1975**, *16*, 85−91.
(72) Bontchev, R. P.; Sevov, S. C. $Co_5BP_3O_{14}$: the First Borophosphate with Planar BO_3 groups connected to PO_4 Tetrahedra. *Inorg. Chem.* **1996**, *35*, 6910−6911.
(73) Wang, Y.; Zhang, B. B.; Yang, Z. H.; Pan, S. L. Cation-Tuned Synthesis of Fluorooxoborates: Towards Optimal Deep-Ultraviolet Nonlinear Optical Materials. *Angew. Chem., Int. Ed.* **2018**, *57*, 2150−2154.
(74) Zhang, Z. Z.; Wang, Y.; Zhang, B. B.; Yang, Z. H.; Pan, S. L. Polar Fluorooxoborate NaB_4O_6F: A Promising Material for Ionic Conduction and Nonlinear Optics. *Angew. Chem., Int. Ed.* **2018**, *57*, 6577.
(75) Liang, F.; Kang, L.; Gong, P. F.; Lin, Z. S.; Wu, Y. C. Rational Design of Deep-Ultraviolet Nonlinear Optical Materials in Fluoroxooborates: Toward Optimal Planar Configuration. *Chem. Mater.* **2017**, *29*, 7098−7102.
(76) Chen, C. T.; Wu, B. C.; Jiang, A. D.; You, G. M. A New-Type Ultraviolet SHG Crystal-Beta-BaB_2O_4. *Sci. Sin. Ser. B* **1985**, *28*, 235−243.
(77) Jiang, X. X.; Luo, S. Y.; Kang, L.; Gong, P. F.; Yao, W. J.; Huang, H. W.; Li, W.; Huang, R. J.; Wang, W.; Li, Y. C.; Li, X. D.; Wu, X.; Lu, P. X.; Li, L. F.; Chen, C. T.; Lin, Z. S. Isotropic Negative Area Compressibility Over Large Pressure Range in Potassium Beryllium Fluoroborate and Its Potential Applications in Deep Ultraviolet Region. *Adv. Mater.* **2015**, *27*, 4851−4857.
(78) Eda, G.; Maier, S. Two-Dimensional Crystals: Managing Light for Optoelectronics. *ACS Nano* **2013**, *7*, 5660−5665.

DOI: 10.1021/acs.inorgchem.8b01712
Inorg. Chem. 2018, 57, 11146−11156